Chemical Science

ROYAL SOCIETY OF CHEMISTRY

EDGE ARTICLE

View Article Online
View Journal | View Issue

Cite this: *Chem. Sci.*, 2024, **15**, 18022

All publication charges for this article have been paid for by the Royal Society of Chemistry

MR-TADF liquid crystals: towards self assembling host–guest mixtures showing narrowband emission from the mesophase†‡

Julius A. Knöller, *[a] Franziska Müller,[a] Tomas Matulaitis, [b] John M. dos Santos, [b] Abhishek Kumar Gupta, [b] Eli Zysman-Colman *[b] and Sabine Laschat *[a]

Received 4th July 2024
Accepted 20th September 2024

DOI: 10.1039/d4sc04429k

rsc.li/chemical-science

Creating (room temperature) liquid crystalline TADF materials that retain the photophysical properties of the monomolecular TADF emitters remains a formidable challenge. The strong intramolecular interactions required for formation of a liquid crystal usually adversely affect the photophysical properties and balancing them is not yet possible. In this work, we present a novel host–guest approach enabling unperturbed, narrowband emission from an MR-TADF emissive core from strongly aggregated columnar hexagonal (Col_h) liquid crystals. By modifying the **DOBNA** scaffold with mesogenic groups bearing alkoxy chains of different lengths, we created a library of Col_h liquid crystals featuring phase ranges >100 K and room temperature mesomorphism. Expectedly, these exhibit broad excimer emission from their neat films, so we exploited their high singlet (S_1 ~2.9 eV) and triplet (T_1 ~2.5 eV) energies by doping them with the MR-TADF guest **BCzBN**. Upon excitation of the host, efficient Förster Resonance Energy Transfer (FRET) resulted in almost exclusive emission from **BCzBN**. The ability of the liquid crystallinity of the host to not be adversely affected by the presence of **BCzBN** is demonstrated as is the localization of the guest molecules within the aliphatic chain network of the host, resulting in extremely narrowband emission (FWHM = 14–15 nm). With this work we demonstrate a strategy for the self-assembly of materials with previously mutually incompatible properties in emissive liquid crystalline systems: strong aggregation in Col_h mesophases, and narrowband emission from a MR-TADF core.

Introduction

Thermally activated delayed fluorescence (TADF), which involves the (up)conversion of triplet excitons (T_1) to singlets (S_1), can be induced in an organic fluorophore through one of two principal distinct molecular designs. First, and more common, are compounds that adopt a strongly twisted donor–acceptor structure (DA-TADF).[1–5] An exciting alternative strategy involves the doping of a polycyclic aromatic hydrocarbon compound with electron-poor atoms/units (B, C=O, P=O) and electron-rich atoms (O, N, S, Se) possessing antagonistic mesomeric effects,[6–9] embodied in so-called multiresonant TADF (MR-TADF) emitters.[10,11] MR-TADF materials are highly sought after as they show narrowband emission and high photoluminescence quantum yields (Φ_{PL}) resulting from their rigid structure.[6–8] Although being employed in many fields from time-resolved luminescence imaging reagents,[12–14] as photosensitizers for solar fuels[14,15] or as photocatalysts for organic transformations,[16,17] TADF compounds are most prominently used as state-of-the-art emitters in organic light emitting diodes (OLEDs).[1–11]

Liquid crystals (LCs) and especially columnar LCs are highly sought after for their anisotropic charge mobility and have thus been heavily investigated in the context of organic electronics.[18–22] In this context, numerous luminescent LCs have been developed as emitter materials for OLEDs.[22–25]

Most recently, TADF liquid crystals (LCs) (TADF-LCs) have emerged as a new class of emitters.[26–31] Several columnar hexagonal (Col_h) TADF-LCs based on an archetypal carbazole-benzonitrile DA-TADF system[1] functionalized with long alkoxy chains **1a–1c** have been developed (Fig. 1).[26,27] Furthermore, smectic derivatives ***p*-DPS-Ac-LC** [28] and ***R*/*S*-4** [30] unit have been reported.[28] MR-TADF skeletons have been employed in the nematic discotic (N_D) **DiKTa-LC** [29] and boron-based Col_h LCs **2** [32] and **BON-LC**.[31]

The distinct self-assembly of TADF-LCs allows for increased charge mobility,[28] improved solution processability,[26–29] controlled alignment of their transition dipoles,[29] and boosted circularly polarized luminescence.[30] While the above-

[a]*Institute of Organic Chemistry, University of Stuttgart, Pfaffenwaldring 55, D-70569, Stuttgart, Germany. E-mail: sabine.laschat@oc.uni-stuttgart.de*

[b]*Organic Semiconductor Centre, EaStCHEM School of Chemistry, University of St Andrews, St Andrews, Fife, KY16 9ST, UK. E-mail: eli.zysman-colman@st-andrews.ac.uk; Fax: +44 (0)1334 463808; Tel: +44 (0)1334 463826*

† In memoriam of Prof. Dr Suning Wang (1958–2020).

‡ Electronic supplementary information (ESI) available. See DOI: https://doi.org/10.1039/d4sc04429k

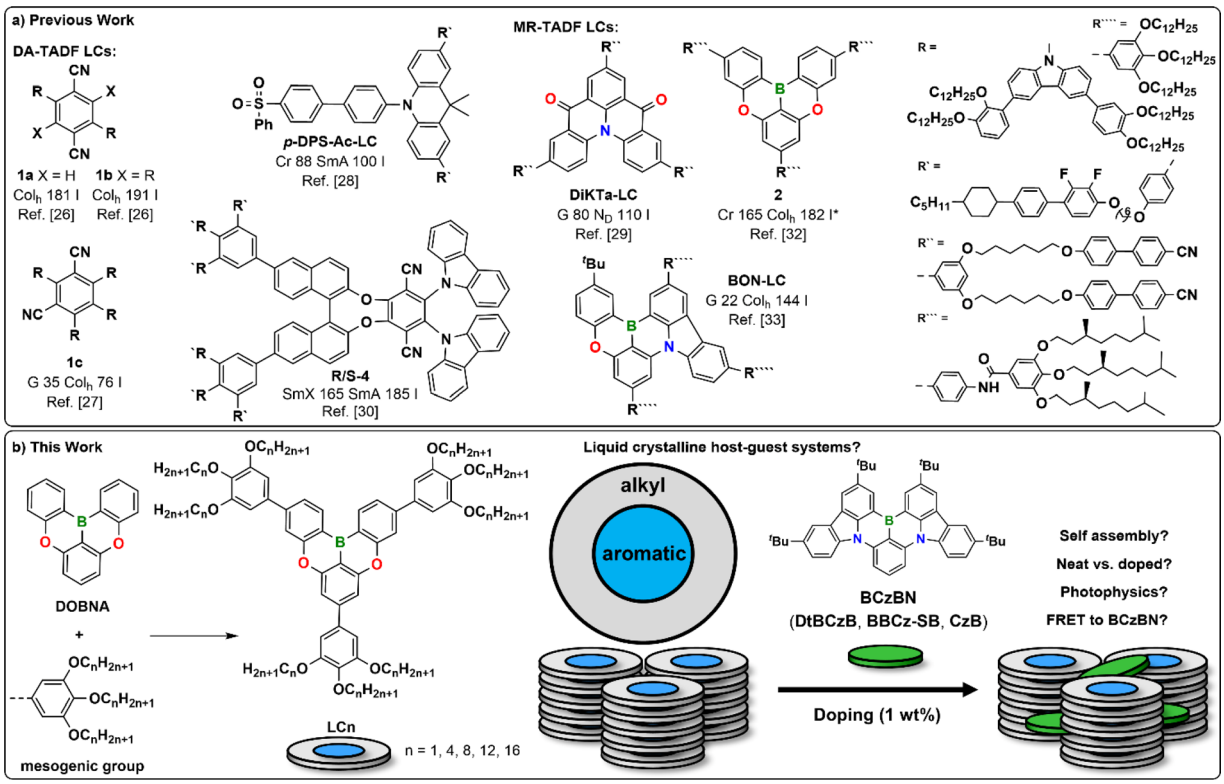

Fig. 1 (a) Previously reported DA-TADF (**1a–1c**, *p*-**DPS-Ac-LC**, *R*/*S*-**4**) and MR-TADF LCs (**DiKTa-LC**, **2**, **BON-LC**); (b) our strategy for development of a liquid crystalline host–guest system based on **LCn** doped with **BCzBN**.

mentioned advantages of TADF-LCs stem from their distinct self-assembly, the strong intramolecular interactions required for LC formation adversely affect their photophysics. TADF-LCs usually display aggregation-caused quenching as well as red-shifted and broadened emission profiles as neat films.[26–31] In other words, the desired self-assembly impairs the photophysical properties of the TADF-LCs. This is especially an issue for MR-TADF based TADF-LCs as both **2** and **BON-LC** display broad excimer emission without a delayed component in their mesophases.[31,32] These effects can be partially suppressed in the low ordered, nematic discotic (N_D) **DiKTa-LC** (Fig. 1).[29] As a countermeasure, TADF-LCs are doped (1–20 wt%) into small molecular or polymeric host materials to suppress undesirable intramolecular interactions,[26–30,33] just as most of their non-LC congeners.[34,35] While this improves their photophysics, the doped systems do not show LC behaviour – undermining the initial effort to develop TADF-LCs. A columnar LC preserving the delicate photophysics of a (prone-to-excimer formation) MR-TADF emitter remains elusive to date.[36–38]

Inspired by reports demonstrating Förster Resonance Energy Transfer (FRET) from liquid crystalline hosts to guest molecules,[39–41] we posited that a MR-TADF based host–guest system would address the outstanding issue of conserving the narrowband emission in the liquid crystalline phase.

Based on **DOBNA**,[10] several high-energy hosts for MR-TADF materials such as **DOBNA-Tol**,[42] have been developed.[42–47] Thus we propose **LCn**, a potentially liquid crystalline host[32] containing this MR-TADF core (Fig. 1b). Decoration of the **DOBNA** [10] core with three mesogenic groups bearing alkoxy chains of different lengths (n = 1, 4, 8, 12, 16) was expected to induce the desired mesomorphic behaviour of **LCn**.[33,48] By doping analogues of **LCn** with the MR-TADF emitter **BCzBN** (aka **DtCzBN**, **BCz-BN**, **Cz-B**),[38,49,50] we demonstrate a liquid crystalline host–guest system that preserves the mesomorphic properties of the **LCn** host and the characteristic narrowband emissive properties of the **BCzBN** guest.

Results and discussion

Theoretical calculations

To understand the impact of the electron-rich mesogenic groups on the photophysical properties of the **DOBNA** core, we modelled all 5 envisioned derivatives of the **LCn** series using time-dependent density functional theory (TD-DFT) at the PBE0/6-31G(d,p) level with the Tamm–Dancoff-approximation (TDA). The highest occupied and lowest unoccupied molecular orbitals, HOMO and LUMO, of each of the **LCn** derivatives are similarly distributed across the MR-TADF cores (Fig. S2‡). While the methyl derivative **LC1** has HOMO/LUMO energies of $E_{HOMO} = -5.82$ eV/$E_{LUMO} = -1.73$ eV, an increase in the alkyl chain length results in a small destabilization of these energies in **LC000**, with E_{HOMO} ranging between −5.64 and −5.66 eV while the LUMO remains essentially the same at $E_{LUMO} = -1.60$ eV (Fig. S2‡). These values are comparable to the ones reported for **DOBNA** ($E_{HOMO} = -5.62$ eV/$E_{LUMO} = -1.66$ eV) computed using B3LYP/6-31G(d), suggesting that the

mesogenic units will only influence slightly the photophysics of the **DOBNA** core as monomolecular systems.[10] Recognizing that state energies are poorly modelled using DFT,[51,52] we modelled a representative example, **LC1**, using double hybrid density functional theory (DH-DFT) at the wPBEPP86/cc-pVDz level to obtain accurate S_1 and T_1 energies (Fig. S1‡).[31,53,54] The difference density plots reveal the characteristic alternating pattern of increasing and decreasing electron density in the S_1 and T_1 states compared to the ground state, while the transition to the S_1 state has a high oscillator strength, *f*, of 0.89. These results are typical for an S_1 state of short-range charge transfer (SRCT) character that is emblematic of MR-TADF emitters.[10,55] The computed S_1 and T_1 energies are $S_1 = 3.76$ eV and $T_1 = 3.44$ eV, resulting in a somewhat large singlet-triplet energy gap, $\Delta E_{ST} = 0.31$ eV.

Synthesis

Due to the promise of these calculations, we proceeded to prepare a family of **LCn** derivatives with chain lengths of $n = 1$, 4, 8, 12, 16 *via* a Suzuki–Miyaura cross-coupling of the pinacol borolanes **3–7** with a brominated **DOBNA** derivative **8** in 38–51% yield (Scheme 1). The identity and purity of the 5 derivatives were determined by a combination of ^{1}H and ^{13}C-NMR spectroscopy and HRMS. The preparation of the aromatic core **8**,[32] the pinacol borolanes **3–7**,[56–59] and the emitter **BCzBN** [38] followed modified literature procedures that are outlined in Schemes S1–S3 and Table S1.‡

Mesomorphic properties

With the materials **LC1–LC16** in hand, we investigated their mesomorphic properties in neat and doped (1 wt% **BCzBN**) powders using polarized optical microscopy (POM), differential scanning calorimetry (DSC) and small angle (SAXS) as well as wide angle X-ray scattering (WAXS) measurements. To our delight, all derivatives except **LC1** (melting point: 291 °C), exhibit mesomorphic behaviour in neat form exemplarily discussed for **LC8**. DSC investigation of **LC8** revealed only a clearing point (T_c) at T_c = 154.6/154.1 °C during heating/cooling, respectively (rate: 10 K min^{-1}), and there were no other apparent phase transitions (Fig. S29c‡). POM measurements revealed that upon cooling from the isotropic phase, **LC8** exhibited fan-shaped textures with line defects (Fig. S28b‡) that could be sheared and vitrified below −20 °C, indicating that it exists as a columnar mesophase. Further, SAXS investigation revealed the (10), (11), (20) and (21) reflections in characteristic $1 : 1/\sqrt{3} : 1/2 : 1/\sqrt{7}$ ratios of a hexagonal lattice (Fig. 2 and ESI, Table S4‡).[60] The wide-angle regime consisted of the superposition of a broad halo ($d_{halo} = 4.43$ Å) and a π–π reflection ($d_{\pi-\pi} = 3.59$ Å), resulting from the molten alkyl chains and the tightly stacked aromatic cores of **LC8**, respectively. Accordingly, **LC8** exists as an enantiotropic Col_h mesophase between −20 and 155 °C, with tightly stacked aromatic cores ($d_{\pi-\pi} = 3.59$ Å) and a lattice parameter (*i.e.*, distance of neighbouring molecules) of $a = 31.4$ Å (Fig. 2a).

The mesophases of the other derivatives **LC4**, **LC12** and **LC16** were analogously assigned as Col_h mesophases (Table S4 and Fig. S31–S34‡), albeit having different transition temperatures

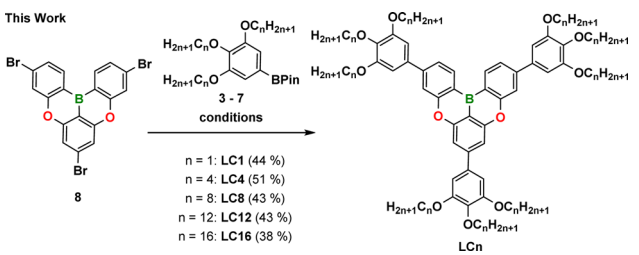

Scheme 1 Synthetic procedure for the preparation of the library of **LCn** compounds possessing different chain lengths varying from $-CH_3$ to $C_{16}H_{33}$. Conditions: $Pd(PPh_3)_4$ (0.15 equiv.), **3–7** (3.5 equiv.), Cs_2CO_3 (5 equiv.), toluene : H_2O (10 : 1, v : v), 110 °C, 18 h.

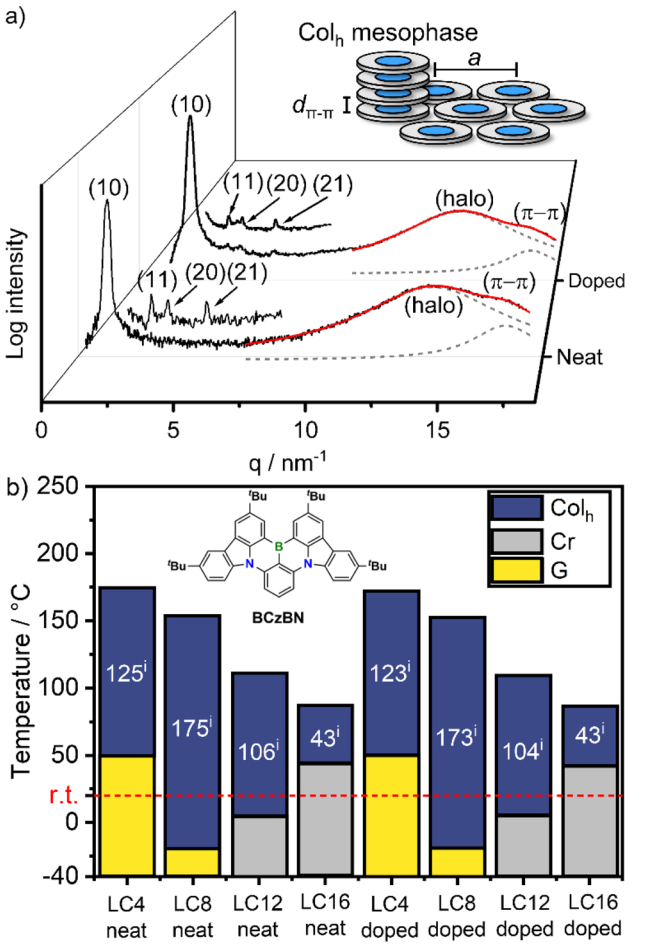

Fig. 2 (a) WAXS diffractograms of **LC8** in neat and doped form (1 wt% **BCzBN**) at 29 °C, also showing magnified SAXS regions. The wide-angle regimes have been fitted (red trace) with two Lorentzian functions (dashed grey traces) for halo- and π–π reflections, respectively, inset shows the schematic assembly of a Col_h mesophase with the π–π distance $d_{\pi-\pi}$ and the lattice parameter *a*; (b) phase behaviour of the mesomorphic **LCn** derivatives in neat and doped (1 wt% **BCzBN**) form (i) phase widths of the Col_h mesophases. Conditions: DSC during cooling (10 K min^{-1}), POM during cooling (1 K min^{-1}), Cr = crystalline, G = glass. For details, please see ESI Tables S3 and S5‡ as well as Fig. S29 and S36.‡

(Fig. 2b). Please note, **LC4** did not show a (20) reflection (Fig.-S31b‡) and **LC12** only displayed the (10) reflection in the SAXS regime (Fig. S33b‡). The mesophases of both DLCs were nonetheless assigned as Col_h: for **LC4** this is due to its characteristic hexagon in the (10) reflection[57] (Fig. S31a‡), while in the case of **LC12** this is due to the characteristic POM textures (Fig. S28c‡). Within the series, the clearing temperatures decreased with increasing chain length from $T_c = 175$ °C (**LC4**) to $T_c = 86$ °C (**LC16**) (Fig. 2b). Both short chain derivatives **LC4** ($T_g = 50$ °C) and **LC8** ($T_g = -20$ °C) vitrified as glasses while the longer chain derivatives **LC12** ($T_m = 5$ °C) and **LC16** ($T_m = 44$ °C) crystallized upon cooling. Consequently, **LC8** exhibited the widest Col_h mesophase with a phase range of 175 °C. Doping of **LC4–LC16** with **BCzBN** (1 wt%) did not alter the Col_h assembly as evident from similar POM textures, DSC traces, and WAXS/SAXS diffractograms (Fig. S35–S40, Tables S5 and S6‡), exemplarily demonstrated from the WAXS pattern of **LC8** (Fig. 2a). As shown in Fig. 2b, doping of each of the **LCn** series with **BCzBN** has no effect on the phase transition temperatures. These findings indicate no significant interaction between **BCzBN** and **LCn** hosts in the mesophase.[61,62]

Optoelectronic properties of LCn

Cyclic voltammetry (CV) and differential pulse voltammetry (DPV) measurements were used to deduce the HOMO/LUMO levels of **LC1–LC16** (Fig. S27‡). From the DPV, oxidation, $E_{ox} =$ 1.25–1.36 V, and reduction potentials *versus* SCE in DCM, $E_{red} =$ −1.81 to −1.73 V, for the **LCn** series were extracted, corresponding to orbital energies of $E_{HOMO} = -6.16$ to −6.05 eV and $E_{LUMO} = -3.04$ to −3.07 eV (Table S2‡). These are slightly stabilized compared to the calculated HOMO/LUMO levels ($E_{HOMO} = -5.82$ to −5.64 eV and $E_{LUMO} = -1.73$ to −1.60 eV). Compared to those of **DOBNA** ($E_{HOMO} = -5.90$ eV, $E_{LUMO} = -2.80$ eV, Table S2 and Fig. S26‡), HOMO and LUMO are slightly stabilized as observed in phenyl-substituted **DOBNA** derivatives.[10]

The photophysical properties of the family of **LCn** derivatives were unsurprisingly found to be very similar. Thus, we discuss the photophysics of **LC8** as a model compound followed by identification of trends in the series.

The absorption spectrum of a toluene solution of **LC8** exhibits two strong bands at $\lambda_{abs} = 340$ nm ($\varepsilon = 3.9 \times 10^4$ M^{-1} L^{-1}) and $\lambda_{abs} = 393$ nm ($\varepsilon = 3.0 \times 10^4$ M^{-1} L^{-1}). The low energy band at $\lambda_{abs} = 393$ nm is associated with the SRCT transition within the substituted **DOBNA** core (Fig. S2‡) and is red-shifted compared to **DOBNA** ($\lambda_{abs} = 376$ nm).[10] The band at $\lambda_{abs} =$ 340 nm is absent in **DOBNA** but is found in phenyl-substituted **DOBNA** derivatives and is thus assigned to a locally excited state of the mesogenic groups of **LC8**.[10]

The photoluminescence (PL) spectrum shows deep blue emission at $\lambda_{PL} = 408$ nm (Fig. 3a). As expected, there is a small Stokes shift $\Delta\bar{\nu} = 1000$ cm^{-1} (15 nm), a narrow full width at half maximum (FWHM) of 24 nm for the PL and a high photoluminescence quantum yield (Φ_{PL}) of 63%, all characteristic of the short-range charge transfer (SRCT) emissive excited state of the **DOBNA** core in **LC8**. The PL band of **LC8** is ∼10 nm

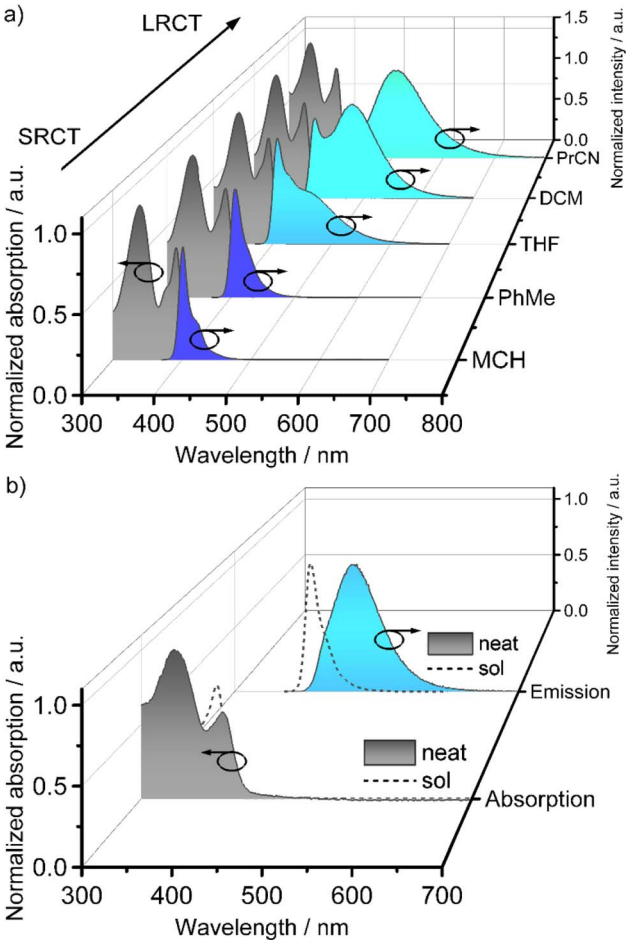

Fig. 3 (a) Normalized absorption (black traces) and PL (blue traces) spectra of **LC8** in solvents of different polarity ($c = 0.02$ mM); (b) absorption (black trace) and PL (blue trace) spectra of a spin-coated film of neat **LC8** in comparison with solution-state spectra in toluene (dashed traces). $\lambda_{exc} = 350$ nm, MCH = methylcyclohexane, PhMe = toluene, THF = tetrahydrofurane, DCM = dichloromethane, PrCN = butyronitrile, SRCT = short-range charge transfer, LRCT = long-range charge transfer.

bathochromically shifted compared to **DOBNA** ($\lambda_{PL} = 398$ nm, $\Phi_{PL} = 72\%$).[10]

The absorption spectra of **LC8** do not show any shift when varying the solvents polarity (Fig. 3a). However, the PL band becomes broader and there is the emergence of a new shoulder peak in the range of 478–503 m with increasing solvent polarity. This reflects the presence of two emissive states, one the SRCT state and the other a long-range charge transfer (LRCT) state that becomes stabilized in more polar solvents, behaviour that has been similarly reported for donor-substituted MR-TADF molecules.[63–65] As with most MR-TADF compounds, **LC8** exhibits only prompt emission in toluene (Fig. S44b‡), with a lifetime (τ_P) of 3.65 ns. From the onsets of the prompt fluorescence and delayed emission spectra in frozen toluene, **LC8** had a S_1 energy of 3.16 eV and a T_1 energy of 2.70 eV, much more stabilized than the calculated values of $S_1 = 3.76$ eV and $T_1 =$ 3.44 eV. The associated ΔE_{ST} of 460 meV (Fig. S44e‡) is likely too large for TADF and also larger than the calculated $\Delta E_{ST} =$

0.31 eV. The large ΔE_{ST} of **LC8** compared to **DOBNA** (S_1 = 3.12 eV, T_1 = 2.97 eV, ΔE_{ST} = 150 meV in frozen EtOH)[10] can be rationalized by the mixed SRCT/LRCT character of the emissive excited state of **LC8** induced through the presence of the electron-rich mesogenic groups.

As expected, the presence of different chain lengths did not influence the solution-state photophysics within the **LCn** series (Table S7‡). All members of the **LCn** series exhibited SRCT emission (λ_{PL} = 407–408 nm) in low polar solvents as well as LRCT emission of increasing intensity in solvents of increasing solvent polarity (Fig. S42–S46, Tables S7 and S8‡). The Φ_{PL} values in toluene ranged between 58–63%, while ΔE_{ST} ranged between 0.44 and 0.46 eV.

Next, we investigated the neat photophysics of the **LCn** series in spin-coated films compared to the dilute toluene solution, the absorption bands of a neat film of **LC8** are slightly broadened and the absorption maxima bathochromically shifted to λ_{abs} = 341 and 399 nm (Fig. 3b). This indicates only a limited number of ground-state intermolecular interactions of the **LC8** molecules despite their tight stacking in the Col_h mesophase as reported for the related LC **2** and **BON-LC**.[32,33] The λ_{PL} of neat **DOBNA-LC8** is bathochromically shifted to 472 nm and the PL spectrum is broadened (FWHM = 70 nm), attributed to excimer emission as also observed for the **DOBNA** based LC **2** and **BON-LC** (Fig. 3b).[32,33] The time-resolved PL decay of the neat film of **LC8** is complex, modelled as triple exponential decay ($\tau_{p,avg}$ = 16.62 ns) and no delayed emission was observed. The S_1 and T_1 energies of **LC8** are 2.92 and 2.55 eV, respectively, resulting in a somewhat smaller ΔE_{ST} of 370 meV compared to the ΔE_{ST} of 460 meV in toluene. Expectedly for excimers, both the S_1 and T_1 energies of the neat film of **LC8** (Fig. S49‡) are lower than those in dilute toluene solution. The Φ_{PL} of neat **LC8** decreased to 19% due to strong aggregation-caused quenching (ACQ).

The photophysics of neat films of the other **LCn** derivatives do not differ much compared to those of **LC8** (ESI, Table S9 and Fig. S47–S51‡). Overall, the photophysics of the neat films of the family of **LCn** compounds compared to those in toluene are dominated by a bathochromically shifted (λ_{PL} = 434–472 nm) and broadened (FWHM = 52–80 nm) excimer emission as discussed in detail for **LC8**. The Φ_{PL} values are lower at Φ_{PL} = 6–22%. None of these derivatives exhibited TADF due to their high ΔE_{ST} = 340–440 meV. The S_1 energies range between 2.91–2.98 eV and the T_1 energies range between 2.50–2.57 eV. These small differences within the neat films can be explained by differences in the individual packing at r.t. and thus the strength of the intermolecular interactions in the excimers.

Optoelectronic properties of LCn doped with BCzBN

Inspired by **DOBNA**-based host materials such as **DOBNA-Tol**, we investigated the **LCn** series as a host materials due to their large S_1 = 2.91–2.98 eV and T_1 = 2.50–2.57 eV levels. We doped the **LCn** series with the MR-TADF emitter **BCzBN** (S_1 = 2.49 eV, T_1 = 2.38 eV in a frozen EtOH matrix[38]). **BCzBN** was chosen as the emitter as there is a large spectral overlap between its absorption with the emission of neat films of the **LCn** series (Fig. S57‡), which is a prerequisite for an efficient Förster Resonance Energy Transfer (FRET) from host (**LCn**) to guest (**BCzBN**). As previously reported, 1 wt% doped films of **BCzBN** in 3,3′-di(9*H*-carbazol-9-yl)-1,1′-biphenyl (*m*CBP) showed bright, sky-blue emission with λ_{PL} = 493 nm, FWHM = 35 nm and Φ_{PL} = 88%,[50] but as a neat film suffers from excimer formation and severe ACQ, reflected in the much lower Φ_{PL} of 32%.[66] Since all materials of the **LCn** series were found to behave similarly, we will discuss the photophysics of **LC8** doped with **BCzBN** (**BCzBN:LC8**) in detail, followed by a discussion of trends within the doping series **BCzBN:LCn**. Excitation of the doped films was set to λ_{exc} = 350 nm, which is a wavelength with almost exclusive absorption through the respective **LCn** host to avoid direct excitation of **BCzBN** (see Fig. S52‡ for qualitative comparison of **LCn** and **BCzBN** absorption).

The PL of **BCzBN:LC8** is narrow (FWHM = 14 nm) and peaks at λ_{PL} = 476 nm, with Φ_{PL} = 41% (Fig. 4a). This band displays the PL characteristics of the **BCzBN** dopant (λ_{PL} = 472 nm, FWHM = 16 nm, 0.02 mM in methylcyclohexane, Fig. S55‡) in a low polarity environment. Compared to the PL characteristics of 1 wt% doped films of **BCzBN** in *m*CBP (λ_{PL} = 493 nm, FWHM = 35 nm, Φ_{PL} = 88%), the emission of 1 wt% **BCzBN:LC8** is blue-shifted, significantly narrowed, and features a lower Φ_{PL}.[50] The excitation energy is thus efficiently transferred from the **LC8** host to the **BCzBN** guest *via* FRET (Fig. 4c); we note that this energy transfer is not quantitative as residual emission from the **LC8** host is apparent as a tiny shoulder at λ_{PL} ~450 nm (Fig. 4a). From the integrals of the PL of the mixture **BCzBN:LC8** and the integral of the scaled PL of the host **LC8**, an observed FRET efficiency, also known as a proximity ratio E_{PR} = 74% has been calculated (Fig. S60 and Table S13‡). We wish to note that the determination of the absolute FRET efficiencies is complicated and E_{PR} thus serves only as a rough estimation for the energy transfer efficiency in **BCzBN:LC8** as it does not account for spectral narrowing (or broadening as is the case in **BCzBN** blends with **LC1** and **LC4**) compared to that of **BCzBN:LC8**.[67]

TCSPC experiments on **BCzBN:LC8** revealed a complex decay with an average prompt lifetime of τ_p = 8.19 ns (triple exponential fit, Fig. S55b‡), comparable to the τ_p = 8.50 ns reported for **BCzBN** in *m*CBP (1 wt%).[50] In addition to the prompt luminescence of **BCzBN:LC8**, investigation *via* multi-channel scaling (MCS) allowed us to detect delayed emission with a delayed lifetime (τ_d) of 108.5 μs under oxygen-free environment. The delayed lifetime component vanishes in the presence of air, hinting at involvement of oxygen-sensitive T_1 states (ESI, Fig. S55c‡). Compared to the 1 wt% doped films of **BCzBN** in *m*CBP (τ_d = 68.8 μs), the τ_d of **BCzBN:LC8** is longer.[50] Temperature-dependent (77–300 K) time-resolved PL decay measurements confirmed the endothermic nature of the delayed emission (Fig. 4b), which is consistent with TADF.[1]

All films of the **BCzBN:LCn** series exhibit narrowband (FWHM = 14–47 nm) emission, originating mainly from the **BCzBN** guest (λ_{PL} = 476–493 nm, Fig. 4d and Table 1). The FRET efficiency E_{PR} = 84–94% was higher for the other mixtures of the **BCzBN:LCn** series (Fig. S60 and Table S13‡). This could result from a decreased distance between host and emitter in the short chain mixtures **BCzBN:LC1** and **BCzBN:LC4** as well as an increased molar concentration of **BCzBN** in the mixtures

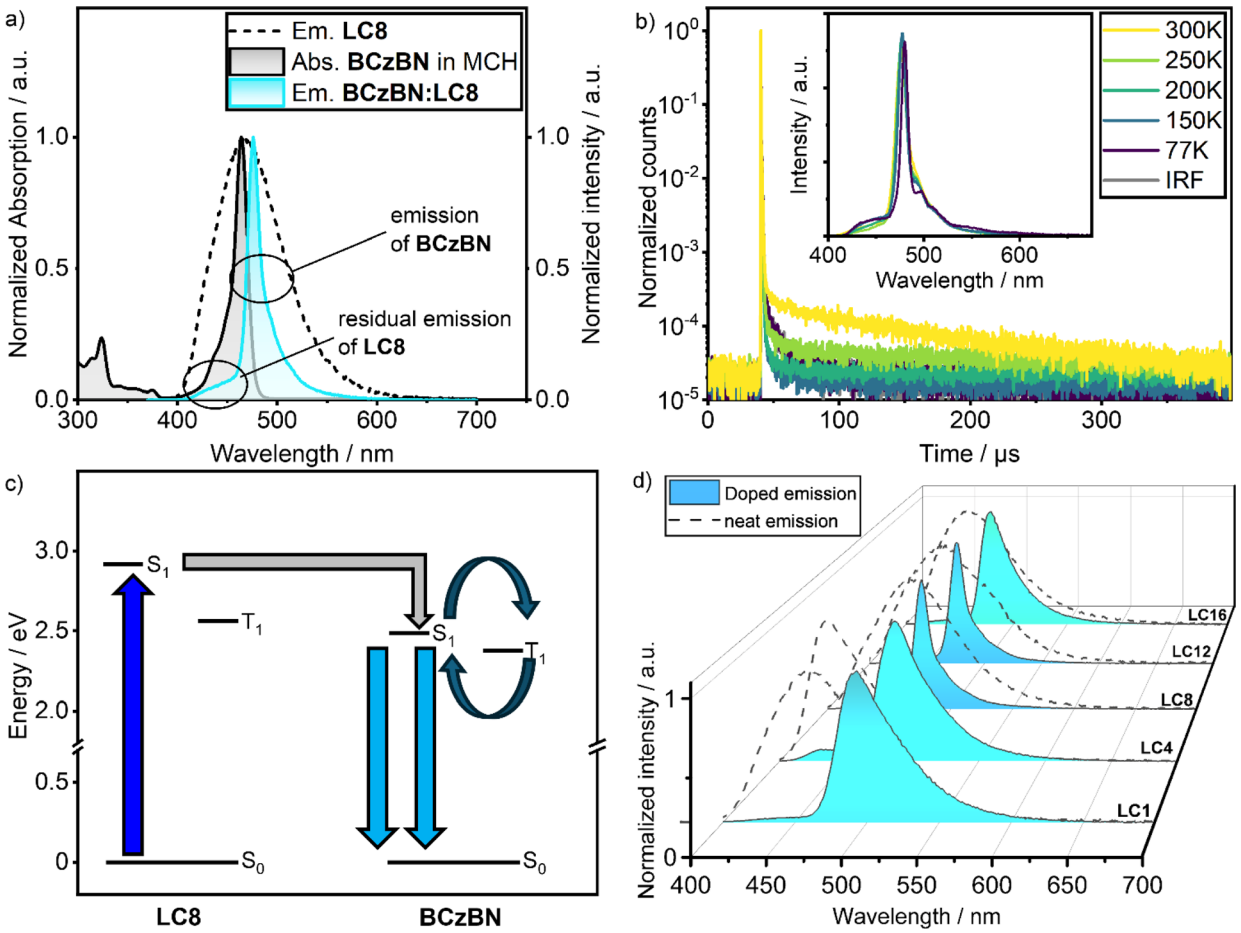

Fig. 4 (a) Steady state emission of **BCzBN** doped in the **LC8** series (1 wt%), neat emission of **LC8** (black dashed trace) and absorption of **BCzBN** in methylcyclohexane (MCH, $c = 0.02$ mM) given for comparison (black trace); (b) temperature dependent lifetime measurements of **LC8** doped with **BCzBN**, inset shows the corresponding steady state emission; (c) emission pathway of **LC8** doped with **BCzBN**; (d) steady state emission of **BCzBN** doped in the **LCn** series ($c = 1$ wt%, blue traces), neat emission of the respective **LCn** derivative given for comparison (black dashed traces). Conditions for films: spin-coated from $CHCl_3$, $c = 1$ wt%, steady state: $\lambda_{exc} = 350$ nm, time resolved: $\lambda_{exc} = 379$ nm.

Table 1 Key photophysical properties of the **LCn** series in neat and doped (1 wt% **BCzBN**) films

#	Conditions	λ_{PL} (FWHM)/nm	Φ_{PL}/%	τ_P[a]/ns	τ_d/µs
LC1	Neat	459 (74)	6	6.98	—
BCzBN:LC1	Doped	493 (47)	33[b]	5.51	—
LC4	Neat	434 (52)	22	6.66	—
BCzBN:LC4	Doped	487 (42)	68[b]	8.03	37.8
LC8	Neat	472 (70)	19	16.62	—
BCzBN:LC8	Doped	476 (14)	41[b]	8.19	108.5
LC12	Neat	463 (88)	19	11.87	—
BCzBN:LC12	Doped	475 (15)	44[b]	4.04	91.5
LC16	Neat	456 (80)	20	9.95	—
BCzBN:LC16	Doped	479 (31)	50[b]	6.46	103.1

[a] Given as amplitude average lifetime. [b] Reflecting Φ_{PL} of **BCzBN** in the respective **LCn** matrix.

BCzBN:LC12 and **BCzBN:LC16**. The other r.t. LC host–guest system, **BCzBN:LC12**, have similar narrowband emission (λ_{PL} = 475 nm, FWHM = 15 nm) compared to **BzCBN:LC8**. While **BCzBN:LC16** has a similar λ_{PL} of 479 nm, its spectrum is broader (FWHM = 31 nm). Both short-chain derivatives **BCzBN:LC1** (λ_{PL} = 493 nm, FWHM = 47 nm) and **BCzBN:LC4** (λ_{PL} = 487 nm, FWHM = 42 nm) show red-shifted and broadened emission compared to **BCzBN:LC8** that are also comparable to the values reported for **BCzBN** in *m*CBP (λ_{PL} = 493 nm, FWHM = 35 nm). Notably, all films of the **BCzBN:LCn** series except for **BCzBN:LC1** show delayed emission, with similar oxygen and temperature dependency as found for **BCzBN:LC8** (Fig. S53–S57‡). The τ_d = 91.5–108.5 µs of the longer chain host–guest blends **BCzBN:LC8**, **BCzBN:LC12** and **BCzBN:LC16** are similar, while **BCzBN:LC4** has a much shorter delayed lifetime of τ_d = 37.8 µs (Table 1). The Φ_{PL} = 68% of **BCzBN:LC4** is higher than for the other mixtures (Φ_{PL} = 33–50%, Table 1). The moderate Φ_{PL} = 41–44% of the rt LC mixtures **BCzBN:LC8** and **BCzBN:LC12** might be explained by the flexible liquid crystalline matrix contributing to non-radiative decay and the non-quantitative FRET (E_{PR} = 74 or 84%). These issues could be addressed by designing a stiffer host LC and by increasing the **BCzBN** concentration to facilitate the energy transfer. Compared to the rt TADF-LCs **1a** (Φ_{PL} = 4%) and **1b** (Φ_{PL} =

20%), our host guest approach shows a markedly improved Φ_{PL} = 41–44%.[26] More importantly, **BCzBN:LC8** and **BCzBN:LC12** conserve the delicate MR-TADF character of **BCzBN** despite the strong aggregation in the Col_h mesophase usually resulting in excimer emission as is the case in **2** and **BON-LC**. Our host–guest approach can thus act as a design principle for liquid crystalline TADF materials having narrowband emission and is not limited to the host LC/emitter combination used in this work.

Packing model of LCn doped with BCzBN

From our investigations of the mesomorphic properties of the **BCzBN:LCn** series, that reveal no influence from the **BCzBN** guest on the mesophase structure, we deduce **BCzBN** to be dispersed in the (liquid) crystalline phases of the respective **DOBNA-LC** host. This finding is supported by the photophysics of the **BCzBN:LCn** series, showing emission from isolated **BCzBN** molecules and no excimer emission from **BCzBN** aggregates or exciplex emission from **DOBNA-BCzBN** assemblies. However, starting from the shortest chain system **BCzBN:LC1** (λ_{PL} = 493 nm, FWHM = 47 nm), the emission bands blue-shift and narrow until reaching a minimum for the r.t. LCs **BCzBN:LC8** (λ_{PL} = 476 nm, FWHM = 14 nm) and **BCzBN:LC12** (λ_{PL} = 475 nm, FWHM = 15 nm). A possible explanation for the blue-shift and narrowing of the emission bands could be that the greater density of the aliphatic chains (Fig. S41‡) leads to a less polar medium experienced by **BCzBN**.[36,68,69] This is also consistent with the fact that the PL of **BCzBN:LC8** (Fig. 5) and **BCzBN:LC12** (Fig. S58b‡) strikingly resemble the emission of **BCzBN** in dilute methylcyclohexane, which implies **BCzBN** being dispersed in a low polar environment in these r.t. LC systems.[68] Columnar liquid crystals such as **LC8** offer such a low polarity environment in form of the alkyl chains (Fig. 5, grey), separating the stacked aromatic cores (Fig. 5, blue, $d_{aromatic}$ = 17.3 Å, DFT calculations) in the mesophase.[19,21] The narrowest distance within the alkyl domain, $d_{alkyl} = d_{molecule} - d_{aromatic}$ = 14.1 Å, can be calculated from the discoid diameter $d_{molecule}$ = 31.4 Å, extracted from the SAXS data ($d_{molecule} = a$). Assuming **BCzBN** as an ellipsoid (green, Fig. 5) with dimensions along the long (d_{long} = 17.2 Å) and short molecular axes (d_{short} = 9.6 Å) extracted from single crystal X-ray diffraction data (CCDC: 2032785),[49] **BCzBN** would geometrically fit into the alkyl domain of **LC8** (Fig. 5).

We thus propose a packing model in which the **BCzBN** guest is dispersed in the alkyl domain of the Col_h mesophase of **BCzBN:LC8**.

A similar packing model is proposed for the **BCzBN:LC12** system (ESI, Fig. S59b‡). The non r.t. LC systems **BCzBN:LC1**, **BCzBN:LC4** and **BCzBN:LC16** exhibit crystalline phases of unknown structure at r.t. and their photophysical behaviour thus cannot be explained by the packing model proposed for **BCzBN:LC8** and **BCzBN:LC12**. The narrowband emission of the **BCzBN:LC1**, **BCzBN:LC4** and **BCzBN:LC16** mixtures identified as emission from the guest **BCzBN**, however, suggests a random dispersion of the **BCzBN** guest in the respective matrices.

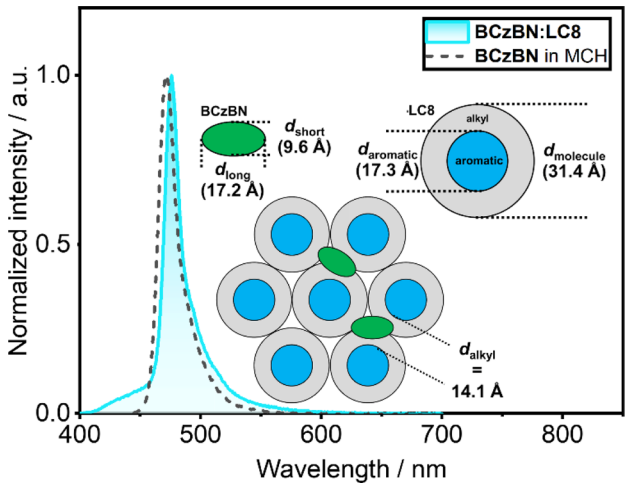

Fig. 5 Normalized emission of **BCzBN** in methylcyclohexane (MCH, 0.02 mM, black dashed trace) and in the **BCzBN:LC8** host–guest system (1 wt%, blue trace). Inset shows a proposed packing model for **BCzBN:LC8** with **BCzBN** assembling in the alkyl chains of **LC8**. The model is derived from SAXS data ($d_{molecule}$ = 31.4 Å), DFT calculations ($d_{aromatic}$ = 17.3) and the single crystal X-ray structure (CCDC: 2032785)[49] of **BCzBN** (d_{long} = 17.2 Å, d_{short} = 9.6 Å).

Conclusions

In summary, we prepared a series of liquid crystalline host materials, **LCn**, based on the MR-TADF **DOBNA** core functionalized with mesogenic groups bearing alkoxy chains of different chain length. Depending on the chain length, these derivatives exhibited Col_h mesophases with phase widths of greater than 100 °C and room temperature mesomorphism. Their neat photophysics is dominated by broad excimer emission due to the strong aggregation required for Col_h formation. When the guest MR-TADF emitter **BCzBN** is added at 1 wt% doping, efficient FRET is observed, allowing for the first time a r.t. LC system that shows narrowband TADF and high Φ_{PL}. Since many of the favourable properties associated with LCs (*e.g.*, charge mobility and boosted chiroptical properties) depend on the presence of a LC phase, this work is an important step to demonstrating the utility of MR-TADF LCs in organic optoelectronics. In a general context, this work outlines a novel host–guest strategy for TADF-LCs that combines both the strong intramolecular interactions required for LC formation with the favourable TADF properties of a dilute emitter. With many host and emitter moieties available for the construction of liquid crystalline host–guest systems, we believe this work will inspire scientists to design new self-assembling materials for solution-processable optoelectronic applications.

Data availability

The research data supporting this publication can be accessed at **https://doi.org/10.17630/7ee54fc1-2819-4d08-a726-439ceab8434c**.

Author contributions

J. A. K. conceived and supervised the project, performed part of the synthesis as well as characterization and wrote the first draft of the manuscript. F. M. performed part of the synthesis and characterization. T. M. and A. K. G. helped with characterization computation and manuscript preparation and J. M. D. S. provided **BCzBN** as well as helped with manuscript preparation. E. Z.-C. and S. L. supervised the project and the manuscript preparation.

Conflicts of interest

There are no conflicts to declare.

Acknowledgements

Generous financial support by the Studienstiftung des deutschen Volkes (PhD fellowship for J. A. K.), the Ministerium für Wissenschaft, Forschung und Kunst des Landes Baden Württemberg, the Carl Schneider Stiftung Aalen (shared instrumentation grant) and the DFG (INST 41/897-1, INST 41/1136-1) are gratefully acknowledged. The St. Andrews team would also like to thank EPSRC (EP/P010482/1 and EP/W007517/1) and the Leverhulme Trust (RPG-2022-032) for financial support. J. A. K. would like to thank Yannick Stöckl and Sofia Hilbers for fruitful discussions.

Notes and references

1 H. Uoyama, K. Goushi, K. Shizu, H. Nomura and C. Adachi, *Nature*, 2012, **492**, 234–238.
2 Z. Yang, Z. Mao, Z. Xie, Y. Zhang, S. Liu, J. Zhao, J. Xu, Z. Chi and M. P. Aldred, *Chem. Soc. Rev.*, 2017, **46**, 915–1016.
3 X. Liang, Z. Tu and Y. Zheng, *Chem. - Eur. J.*, 2019, **25**, 5623–5642.
4 Y. Liu, C. Li, Z. Ren, S. Yan and M. R. Bryce, *Nat. Rev. Mater.*, 2018, **3**, 18020.
5 J. Shi, Z. Ran, F. Peng, M. Chen, L. Li, L. Ji and W. Huang, *J. Mater. Chem. C*, 2022, **10**, 9165–9191.
6 S. Madayanad Suresh, D. Hall, D. Beljonne, Y. Olivier and E. Zysman-Colman, *Adv. Funct. Mater.*, 2020, **30**, 1908677.
7 Y. Xu, Q. Wang, X. Cai, C. Li, S. Jiang and Y. Wang, *Angew. Chem., Int. Ed.*, 2023, e202312451.
8 H. J. Kim and T. Yasuda, *Adv. Opt. Mater.*, 2022, **10**, 2201714.
9 H. Zhang, G. Li, X. Guo, K. Zhang, B. Zhang, X. Guo, Y. Li, J. Fan, Z. Wang, D. Ma and B. Z. Tang, *Angew. Chem., Int. Ed.*, 2021, 202108540.
10 H. Hirai, K. Nakajima, S. Nakatsuka, K. Shiren, J. Ni, S. Nomura, T. Ikuta and T. Hatakeyama, *Angew. Chem., Int. Ed.*, 2015, **54**, 13581–13585.
11 T. Hatakeyama, K. Shiren, K. Nakajima, S. Nomura, S. Nakatsuka, K. Kinoshita, J. Ni, Y. Ono and T. Ikuta, *Adv. Mater.*, 2016, **28**, 2777–2781.
12 N. R. Paisley, C. M. Tonge and Z. M. Hudson, *Front. Chem.*, 2020, **8**, 229.
13 V.-N. Nguyen, A. Kumar, M. H. Lee and J. Yoon, *Coord. Chem. Rev.*, 2020, **425**, 213545.
14 W. Chen and F. Song, *Chin. Chem. Lett.*, 2019, **30**, 1717–1730.
15 A. M. Polgar and Z. M. Hudson, *Chem. Commun.*, 2021, **57**, 10675–10688.
16 M. A. Bryden and E. Zysman-Colman, *Chem. Soc. Rev.*, 2021, **50**, 7587–7680.
17 R. Hojo, A. M. Polgar and Z. M. Hudson, *ACS Sustainable Chem. Eng.*, 2022, **10**, 9665–9678.
18 R. De and S. K. Pal, *Chem. Commun.*, 2023, **59**, 3050–3066.
19 T. Wöhrle, I. Wurzbach, J. Kirres, A. Kostidou, N. Kapernaum, J. Litterscheidt, J. C. Haenle, P. Staffeld, A. Baro, F. Giesselmann and S. Laschat, *Chem. Rev.*, 2016, **116**, 1139–1241.
20 S. Sergeyev, W. Pisula and Y. H. Geerts, *Chem. Soc. Rev.*, 2007, **36**, 1902.
21 J. Uchida, B. Soberats, M. Gupta and T. Kato, *Adv. Mater.*, 2022, **34**, 2109063.
22 R. K. Gupta and A. A. Sudhakar, *Langmuir*, 2019, **35**, 2455–2479.
23 R. De, S. Sharma, S. Sengupta and S. Kumar Pal, *Chem. Rec.*, 2022, **22**, e202200056.
24 T. Hassheider, S. A. Benning, H.-S. Kitzerow, M.-F. Achard and H. Bock, *Angew. Chem., Int. Ed.*, 2001, **40**, 2060–2063.
25 L. G. Franca, P. L. dos Santos, P. Pander, M. G. B. Cabral, R. Cristiano, T. Cazati, A. P. Monkman, H. Bock and J. Eccher, *ACS Appl. Electron. Mater.*, 2022, **4**, 3486–3494.
26 A. F. Suleymanova, M. Z. Shafikov, A. C. Whitwood, R. Czerwieniec and D. W. Bruce, *J. Mater. Chem. C*, 2021, **9**, 6528–6535.
27 A. F. Suleymanova, M. Z. Shafikov, X. Chen, Y. Wang, R. Czerwieniec and D. W. Bruce, *Phys. Chem. Chem. Phys.*, 2022, **24**, 22115–22121.
28 Y. Zhu, S. Zeng, B. Li, A. J. McEllin, J. Liao, Z. Fang, C. Xiao, D. W. Bruce, W. Zhu and Y. Wang, *ACS Appl. Mater. Interfaces*, 2022, **14**, 15437–15447.
29 D. Chen, F. Tenopala-Carmona, J. A. Knöller, A. Mischok, D. Hall, S. Madayanad Suresh, T. Matulaitis, Y. Olivier, P. Nacke, F. Gießelmann, S. Laschat, M. C. Gather and E. Zysman-Colman, *Angew. Chem., Int. Ed.*, 2023, **62**, e202218911.
30 B. He, Q. Zhong, Q. Dong, X. Yang, S. J. Cowling, W. Qiao, D. W. Bruce, W. Zhu, P. Duan and Y. Wang, *Mater. Horiz.*, 2024, **11**, 1251–1260.
31 J. A. Knöller, B. Sönmez, T. Matulaitis, A. K. Gupta, E. Zysman-Colman and S. Laschat, *Chem. Commun.*, 2024, **60**, 4459–4462.
32 B. Adelizzi, P. Chidchob, N. Tanaka, B. A. G. Lamers, S. C. J. Meskers, S. Ogi, A. R. A. Palmans, S. Yamaguchi and E. W. Meijer, *J. Am. Chem. Soc.*, 2020, **142**, 16681–16689.
33 J. A. Knöller, B. Sönmez, T. Matulaitis, A. K. Gupta, E. Zysman-Colman and S. Laschat, *Chem. Commun.*, 2024, **60**, 4459–4462.
34 N. Li, F. Ni, X. Lv, Z. Huang, X. Cao and C. Yang, *Adv. Opt. Mater.*, 2022, **10**, 2101343.
35 T. Chatterjee and K.-T. Wong, *Adv. Opt. Mater.*, 2019, **7**, 1800565.

36 K. Stavrou, A. Danos, T. Hama, T. Hatakeyama and A. Monkman, *ACS Appl. Mater. Interfaces*, 2021, **13**, 8643–8655.
37 Y. Yuan, X. Tang, X. Du, Y. Hu, Y. Yu, Z. Jiang, L. Liao and S. Lee, *Adv. Opt. Mater.*, 2019, **7**, 1801536.
38 S. Xu, Q. Yang, Y. Zhang, H. Li, Q. Xue, G. Xie, M. Gu, J. Jin, L. Huang and R. Chen, *Chin. Chem. Lett.*, 2021, **32**, 1372–1376.
39 A. C. A. Chen, S. W. Culligan, Y. Geng, S. H. Chen, K. P. Klubek, K. M. Vaeth and C. W. Tang, *Adv. Mater.*, 2004, **16**, 783–788.
40 S.-H. Liu, M.-S. Lin, L.-Y. Chen, Y.-H. Hong, C.-H. Tsai, C.-C. Wu, A. Poloek, Y. Chi, C.-A. Chen and S. H. Chen, *Org. Electron.*, 2011, **12**, 15–21.
41 Y. Wu, C. Yan, X. Li, L. H. You, Z. Yu, X. Wu, Z. Zheng, G. Liu, Z. Guo, H. Tian and W. Zhu, *Angew. Chem., Int. Ed.*, 2021, **60**, 24549–24557.
42 S. Oda, W. Kumano, T. Hama, R. Kawasumi, K. Yoshiura and T. Hatakeyama, *Angew. Chem., Int. Ed.*, 2021, **60**, 2882–2886.
43 Y. Sano, T. Shintani, M. Hayakawa, S. Oda, M. Kondo, T. Matsushita and T. Hatakeyama, *J. Am. Chem. Soc.*, 2023, **145**, 11504–11511.
44 S. Oda, T. Sugitani, H. Tanaka, K. Tabata, R. Kawasumi and T. Hatakeyama, *Adv. Mater.*, 2022, 2201778.
45 S. Oda, B. Kawakami, R. Kawasumi, R. Okita and T. Hatakeyama, *Org. Lett.*, 2019, **21**, 9311–9314.
46 Y. Kondo, K. Yoshiura, S. Kitera, H. Nishi, S. Oda, H. Gotoh, Y. Sasada, M. Yanai and T. Hatakeyama, *Nat. Photonics*, 2019, **13**, 678–682.
47 S. Park, H. Kwon, H. Lee, K. Lee, S. Kang, K. J. Kim, T. Kim and J. Park, *J. Mater. Chem. C*, 2024, **12**, 4384–4391.
48 T. Kushida, A. Shuto, M. Yoshio, T. Kato and S. Yamaguchi, *Angew. Chem., Int. Ed.*, 2015, **54**, 6922–6925.
49 M. Yang, I. S. Park and T. Yasuda, *J. Am. Chem. Soc.*, 2020, **142**, 19468–19472.
50 Y. Xu, Z. Cheng, Z. Li, B. Liang, J. Wang, J. Wei, Z. Zhang and Y. Wang, *Adv. Opt. Mater.*, 2020, **8**, 1902142.
51 A. Pershin, D. Hall, V. Lemaur, J.-C. Sancho-Garcia, L. Muccioli, E. Zysman-Colman, D. Beljonne and Y. Olivier, *Nat. Commun.*, 2019, **10**, 597.
52 D. Hall, J. C. Sancho-García, A. Pershin, G. Ricci, D. Beljonne, E. Zysman-Colman and Y. Olivier, *J. Chem. Theory Comput.*, 2022, **18**, 4903–4918.
53 T. Schwabe and S. Grimme, *Phys. Chem. Chem. Phys.*, 2007, **9**, 3397.
54 M. Kondo, *Chem. Phys. Lett.*, 2022, **804**, 139895.
55 Y. Zhang, D. Zhang, J. Wei, Z. Liu, Y. Lu and L. Duan, *Angew. Chem., Int. Ed.*, 2019, **58**, 17068–17073.
56 T. Yasuda, T. Shimizu, F. Liu, G. Ungar and T. Kato, *J. Am. Chem. Soc.*, 2011, **133**, 16912–16917.
57 T. Wöhrle, S. J. Beardsworth, C. Schilling, A. Baro, F. Giesselmann and S. Laschat, *Soft Matter*, 2016, **12**, 3730–3736.
58 S. Sugiura, W. Matsuda, W. Zhang, S. Seki, N. Yasuda and H. Maeda, *J. Org. Chem.*, 2019, **84**, 8886–8898.
59 Y. Haketa, S. Sakamoto, K. Chigusa, T. Nakanishi and H. Maeda, *J. Org. Chem.*, 2011, **76**, 5177–5184.
60 N. Godbert, A. Crispini, M. Ghedini, M. Carini, F. Chiaravalloti and A. Ferrise, *J. Appl. Crystallogr.*, 2014, **47**, 668–679.
61 K. Praefcke and J. D. Holbrey, *J. Inclusion Phenom. Macrocyclic Chem.*, 1996, **24**, 19–41.
62 M. Ebert, G. Frick, Ch. Baehr, J. H. Wendorff, R. Wüstefeld and H. Ringsdorf, *Liq. Cryst.*, 1992, **11**, 293–309.
63 S. Wu, W. Li, K. Yoshida, D. Hall, S. Madayanad Suresh, T. Sayner, J. Gong, D. Beljonne, Y. Olivier, I. D. W. Samuel and E. Zysman-Colman, *ACS Appl. Mater. Interfaces*, 2022, **14**, 22341–22352.
64 J. A. Knöller, G. Meng, X. Wang, D. Hall, A. Pershin, D. Beljonne, Y. Olivier, S. Laschat, E. Zysman-Colman and S. Wang, *Angew. Chem., Int. Ed.*, 2020, **59**, 3156–3160.
65 Z. Huang, H. Xie, J. Miao, Y. Wei, Y. Zou, T. Hua, X. Cao and C. Yang, *J. Am. Chem. Soc.*, 2023, **145**, 12550–12560.
66 Y. Zhang, J. Wei, D. Zhang, C. Yin, G. Li, Z. Liu, X. Jia, J. Qiao and L. Duan, *Angew. Chem., Int. Ed.*, 2022, **61**, e202113206.
67 J. J. McCann, U. B. Choi, L. Zheng, K. Weninger and M. E. Bowen, *Biophys. J.*, 2010, **99**, 961–970.
68 B. Bardi, D. Giavazzi, E. Ferrari, A. Iagatti, M. Di Donato, D. K. A. Phan Huu, F. Di Maiolo, C. Sissa, M. Masino, A. Lapini and A. Painelli, *Mater. Horiz.*, 2023, **10**, 4172–4182.
69 C. F. Madigan and V. Bulović, *Phys. Rev. Lett.*, 2003, **91**, 247403.